

Evidence of Fermi acceleration of Lyman α in the Radio Galaxy 1243+036¹

Luc Binette², Benoit Joguet³ and John C. L. Wang⁴

binette@astroscu.unam.mx, bjoguet@eso.org, jcwang@astro.umd.edu

ABSTRACT

The high redshift radiogalaxy 1243+036 ($z = 3.6$) presents an asymmetric Ly α profile of FWHM 1550 km s^{-1} as measured by van Ojik et al. We propose that the blue asymmetry in the Ly α profile is not due to narrow absorption dips but consists of narrow emission peaks. We interpret the blueshifted peaks near -1130 , -850 and -550 km s^{-1} (relative to the peak of full profile) as being the result of Fermi acceleration of Ly α produced by jet-induced star formation in the wake of a 300 km s^{-1} shock. This shock would be caused by the deflection of the radio-jet at the observed position of the radio bend which also coincides spatially with the excess Ly α emission reported by van Ojik et al.

Subject headings: galaxies: individual (1243+036) — galaxies: jet — physical data and processes: shock waves — line: formation — line: profiles

¹Based on NTT observations archived at the European Southern Observatory: <http://arch-http.hq.eso.org/>

²Instituto de Astronomía, UNAM, Ap. 70264, 04510 México, DF, México

³European Southern Observatory, Casilla 19001, Santiago 19, Chile

⁴Astronomy Department, University of Maryland, College Park, MD 20742-2421, USA

1. Introduction

Lyman α is the strongest line observed in very high redshift radio galaxies (HZRG). Although the brightness of Ly α peaks near or at the nuclear position, most of the emission is spatially resolved with the fainter emission extending up to radii 40–130 kpc. The Ly α profile in HZRG is characterized by a FWHM in the range 700–1600 km s $^{-1}$ (van Ojik 1995 and references therein). The intermediate resolution study of Ly α profiles carried out by van Ojik et al. (1997) has revealed the presence of troughs which are well explained by H I gas absorption present in the environment of the parent radio galaxy. In their sample, however, the HZRG 1243+036 ($z = 3.6$) may call for a different interpretation, namely that the broad profile presents true narrow emission features in between the narrow ‘dips’ which van Ojik et al. (1996: vO96) have interpreted as absorption features. The repeated scattering of the resonance Ly α line across a shock discontinuity was shown by Neufeld & McKee (1988: NM88) to result in a systematic blueshift of Ly α . In this paper, we develop in more detail the Fermi acceleration model and propose that the narrow features observed by vO96 correspond to a small number of across-shock scatterings.

2. The model

The calculations of the Ly α profile is carried out in two steps. First we compute the emergent profile from the ionized gas, second we consider the effect of Fermi acceleration across a shock discontinuity which is taking place between the observer and the Ly α emission gas.

2.1. Double-horned source profile

A resonant photon escaping from a static slab will diffuse in frequency and space until it can escape in the wings of the opacity profile. This leads to a symmetric double-horned profile with a separation, v_{sep} , between the two peaks of:

$$v_{sep} \approx 390 \left(N_{21}^{sou} \sqrt{T_2^{sou}} \right)^{1/3} \text{ km s}^{-1}, \quad (1)$$

where $10^{21} N_{21}^{sou} \text{ cm}^{-2}$ is the neutral hydrogen column density surrounding the emitting ionized gas and $10^2 T_2^{sou} \text{ K}$ its temperature. We properly take into account the skewness at large N_{21}^{sou} of the two emission peaks (cf. Bonilha et al. 1979) by using the numerical prescription described in Appendix B of Binette et al. (1993). We can either assume the ionized gas to be homogeneous and isothermal (structure-less) or we can integrate the Ly α profile escaping a cooling shock slab or a stratified photoionized slab. In either case, we assume a plane-parallel geometry for the transfer which allows two possible perspectives for an external observer: front or back. The front perspective corresponds to the precursor side (shock wave case) or the UV source side (photoionization case). The fraction of Ly α escaping towards the front or the back can be quite different, especially for an ionization bounded photoionized slab or for a shock wave with a trailing thick shell. The H I gas beyond the Strömgren boundary or within the trailing shell acts like mirrors which favor Ly α photons to escape overwhelmingly towards the front. This effect as well as Ly α destruction due to internal dust are fully taken into account using the formalism developed in Appendix A of Binette et al. (1993). We label N_{21}^{mir} the column density of the trailing H I shell.

2.2. Fermi acceleration of resonant photons

As for the effect of Fermi acceleration on the Ly α profile, unless stated otherwise we will consider the front perspective whereby the shock discontinuity is taking place between the observer and the region producing the line. This is different from the (back) perspective⁵ in NM88 in

⁵Our front perspective prevents the components (a) and (b) discussed in NM88 from being visible.

which the shock was on the far-side of the emergent Ly α (see their Fig. 1). As in NM88, we treat the slabs of scattering material on either side of the shock front N_{21}^{prec} and N_{21}^{mir} as two converging, partially reflecting mirrors. Each passage of a resonant photon across the shock front corresponds to a reflection and, for an isotropic radiation field, the mean blueshift after n passages across the discontinuity is $nV_s/2$, where V_s is the shock wave velocity. If the transmissivity of the mirrors on the k th reflection is T_k and the reflectivity is $1 - T_k$, the fraction of resonant photons escaping at exactly n shock crossings is

$$f(n) = T_n \prod_1^{n-1} (1 - T_k) \approx T_n \exp\left(-\int_0^n T_k dk\right). \quad (2)$$

The right term is a valid approximation only in the limit of large n and $T_k \ll 1$. Unlike NM88, we have used instead the middle term in which each crossing of the discontinuity is calculated following the algorithm described in Appendix A. The main advantage is that it allows us to cover the case of a small number of reflections. Furthermore, it retains higher resolution of the spectral features appearing on the transmitted profile and it allows a more accurate treatment of the effect of dust absorption (see Appendix A). We define μ_D as the dust-to-gas ratio relative to the local interstellar value.

The profile of non-resonant lines of species i of atomic mass m_i are assumed gaussian with a FWHM given by $1.665 (2kT/m_i + v_{turb}^2)^{1/2}$ where v_{turb} is the local ‘most probable’ turbulent velocity. This summarizes the implementation of profile determination in the multipurpose code MAPPINGS IC (cf. Ferruit et al. 1997).

2.3. Profiles produced by Fermi acceleration

To illustrate the type of profiles obtained, we have made calculations under a wide range of input parameters. In these calculations, the shock

velocity, $100 V_7^s \text{ km s}^{-1}$, is constant at $V_7^s = 3.0$. Increasing V_7^s does not necessarily change the shape of profile if the opacities are increased accordingly (although it does blueshift the profile further). For definiteness, we have set $N_{21}^{prec} = N_{21}^{mir}$ in all our calculations⁶. We adopted a temperature of 100 K for the gas responsible for the scattering. The choice of temperature impacts only on v_{sep} [see equation (1)] and therefore only the product $N_{21}^{sou} \sqrt{T_2^{sou}}$ matters to the calculations. At constant temperature, the two essential free parameters are therefore N_{21}^{mir} ($= N_{21}^{prec}$) and N_{21}^{sou} [the column depth immediately surrounding the ionized gas, see equation (1)]. The different profiles resulting from Fermi acceleration are presented in Fig. 1 and the corresponding input parameters in Table 1. It is seen from Fig. 1 that the higher N_{21}^{mir} , the higher the blueshift of the emergent Fermi profile (see Appendix B for a comparison with NM88). v_{sep} is an important factor governing the appearance of the profile when it is $\gtrsim V_s$. The effect of dust on Fermi acceleration is not as severe as in NM88. The main reason is that we considered only the effects of dust within the two mirrors and its implication on the Fermi profile *per se* while disregarding the presence of dust within N_{21}^{sou} , the gas immediately surrounding the source. In any event, little dust absorption would take place when N_{21}^{sou} is small, a possibility strongly favored in the discussion below. Also we expect the extremely hot postshock gas surrounding the embedded condensations to be devoid of dust. In our calculations of the dust effects on the Fermi profile, we have taken into account the mean geometrical depth traversed at each shock crossing by the resonant photon. Fig. 1*j* illustrates the case with $\mu_D = 0.2$ (dust content of mirrors only) which should be compared with the dustfree case of Fig. 1*i*.

⁶In the event of a large imbalance, clearly Ly α would escape in the direction of the thinnest of the two mirrors.

3. Analysis of the 1243+036 data

We have reduced the ESO archived observations of PKS B1243+036 taken at the NTT with EMMI by vO96 on 14 April 1994. The 4 one hour duration long-slit spectra with PA=152° (aligned with the radio axis) were registered on a 2048 × 2048 Tektronix CCD. The 2 × 2 binning gave a spatial scale of 0.54"pix⁻¹. Grating 6 was used with a wide slit of 2.5". Our analysis of the arc spectra indicates a resolution (FWHM) of $\simeq 2.6\text{\AA}$.

After performing a flat-field division, sky subtraction, flux calibration and correction for atmospheric extinction using the IRAF reduction package, we extracted a one-dimensional spectrum using a restricted window of 7", centered on the bending point of the radio source (cf. Fig. 4 and 14 of vO96). The resulting spectrum is plotted as solid line in the upper frame of Fig. 2. It differs from that of vO96 as a result of considering a window which is both smaller and centered around the radio bend.

Several small peaks (present in the individual exposures) appear on the Ly α profile at 5536, 5541 and 5547 \AA . In order to isolate these features, we smoothed the spectrum and subtracted the result from the original spectrum. The result is plotted as a dotted line in the upper frame of Fig. 2. Obviously, the negative part of this curve is unphysical whether the features are emission peaks or absorption dips. To remedy this, we supposed that the underlying Ly α profile is intrinsically symmetric since almost all the Ly α profiles measured by van Ojik et al. (1997) turned out to be symmetric *after* correction of the absorption troughs. Taking the red side of the *smoothed* profile as our reference, we folded it around the peak position ($\lambda_{Max} = 5557.2\text{\AA}$) over the blue side and subtracted it from the original profile. The resulting spectrum is shown in the lower frame of Fig. 2 (dotted line).

4. Fermi acceleration in 1243+036 ?

Are the high frequency features (dotted line in Fig. 2b) absorption dips or emission peaks? The absorption interpretation is ambiguous because the V-shaped dips are unresolved in wavelength, i.e., their widths are less than the width of the flat-topped instrumental profile. This can be seen in Fig. 2b where the instrumental profile is shown in the inset box. On the other hand, if interpreted as emission features, these features appear to fit well the instrumental profile, as is evident from Fig. 2b. Furthermore, the peaks are equally spaced in wavelength and considerably blue shifted relative to systemic velocity, all in accordance with Fermi acceleration. Clearly, higher spatial and spectral resolution spectra would help settle the question. The existence of a shock is not in doubt, however, since 1243+036 clearly shows the presence of a radio bend at a distance of 2" from the nucleus (13.6 kpc for $H_0 = 50 \text{ km s}^{-1}\text{Mpc}^{-1}$ and $q_0 = 0.5$), that is at the same spatial position where vO96 reports genuine enhanced Ly α emission (underlying their absorption dips).

Let us thereafter assume that the narrow emission peaks are independent from the underlying symmetric Ly α profile and that they are emitted near or at the radio bend. Between successive peaks, two reflections must necessarily take place. Therefore the velocity of the shock in our model is fixed by the distance between peaks which gives $V_7^s \simeq 3.0$. If the emission peaks corresponded to gas photoionized by the nucleus, we could *not* explain these by Fermi acceleration since one of the necessary H I mirrors (at the back) could not exist between the ionized gas and the source. Our Fermi acceleration model therefore requires *in situ* photoionization, either by the shock itself (a) or by an independent local source (b).

In case a, the post-shock temperature is of order $1.5 \times 10^6 \text{ K}$ and in order to reproduce the integrated luminosity of the emission features

$(2.4 \times 10^{43} \text{ erg s}^{-1})$, one requires the uncomfortably high pre-shock density of $n_0 = 3 \times 10^6 \text{ cm}^{-3}$ for a shock front area as large as 10^4 pc^2 (we included the ionizing photons generated within the shocked gas). Furthermore, the abundances of the heavy elements must be extremely low since C IV is absent from the spectra (vO96). When we compute the Ly α profile from a shock, it turns out significantly wider (after convolution) than the observed narrow peaks.

In case b, Ly α emission originates from starbursts triggered by the passing of the shock wave which is the result of the deflection of the radio jet. This possibility goes along the suggestion of Rees (1989) that enhanced star formation can be triggered by the interaction of the radio jet with the environment of HZRG. By inspection of many profiles such as in Fig. 1, two possibilities arise. One is that the H II gas is embedded in thick neutral gas such that v_{sep} is equal to V_s . In this particular case, the convolved emission peaks are sufficiently narrow. Such a model is shown in Fig. 1l and it gives, after convolution, an excellent fit. A less *ad hoc* situation which does not rely on having $v_{sep} = V_s$ is to have the H II regions *not* fully embedded but rather in their champagne phase (Tenorio-Tagle 1979). This geometry which facilitates considerably the escape of Ly α into the surrounding shocked gas results in a small v_{sep} . Such a nebular model was computed using a stellar atmosphere model of 40 000 K. The Fermi profile obtained gives an encouraging fit as shown by the solid line in Fig. 2b. It was computed using $V_7^s = 3.0$ and $N_{21}^{mir} = 1.3$ and has a very similar profile to the simpler model of Fig. 1k when the latter is convolved. A point in favor of the Fermi interpretation is that the peaks appear at $-4, -3, -2 V_s$ relative to the adopted value of line center at 1.3 \AA ($70 \text{ km s}^{-1} \simeq \frac{1}{4} V_s$) to the red of λ_{MAX} , while absorption dips ought to be distributed randomly in velocity space.

It is interesting to note that the shock crossing time across a projected distance of $0.2''$ –an upper limit to the projected radio hot spot size– is

$\sim 4 \times 10^6$ years. Incidentally, a preshock gas density of 0.16 cm^{-3} [eight times higher than in Rees 1989] with a column of $N_{21}^{mir} = 1.3$ possess a geometrical depth of $0.2''$. After being shocked, such gas would cool on a timescale of $\sim 0.8 \times 10^6$ years from a postshock temperature of 1.5×10^6 K. If the flow became very chaotic after the gas has cooled, this might preserve a small value for v_{sep} even if the H II regions were to turn on at a later stage further downstream.

Interestingly, the only other candidate HZRG for which Fermi acceleration was proposed, 3C326.1 (NM88), is similarly devoid of C IV emission, a fact difficult to reconcile with either nuclear photoionization by a powerlaw or with high velocity (photoionizing) shocks. Jet-triggered star formation as we argued for above would solve this conundrum since C IV is then expected to be very weak even for solar metallicity.

We wish to thank Huub Röttgering for directing us to the archived NTT data of 1243+036 which were reduced a second time by one of us (BJ). We also thank Irapuan Rodrigues de Oliveira for an initial quick survey on the type of profiles produced by Fermi acceleration. One of us (JCLW) acknowledges support by NASA Astrophysics Theory Program grant NAG5-3836 and by a Graduate Research Board award from the University of Maryland.

A. Numerical algorithm to calculate Fermi profiles

We discretize all profiles in vectors whose indices are proportional to the velocity shift ($v_i = i \delta v$) from line center λ_0 . δv is a proportionality constant sufficiently small to allow fair sampling of the source profile. The source line profile emergent at the shock discontinuity is defined as $\varphi(v_i)$ (cf. § 2.1). It is centered and symmetric around $v_i = 0$. In this scheme, the observer is either on the side of the precursor ('front' perspective): $p = +1$, or downstream beyond the trail-

ing H I shell ('back' perspective): $p = -1$. After $j+1$ passage across the discontinuity of the photons coming from position v_i in the source profile, their *contribution* to the observed profile $\varphi^p(v_k)$ for an observer whose perspective is $p = (-1)^j$ is given by:

$$\varphi(v_i)T(v_j) \prod_{n=0}^{j-1} (1 - T(v_n)) , \quad (\text{A1})$$

where k is the nearest integer to $v_j/\delta v$, and with v_j and v_n given by:

$$v_j = v_i - jV_s/2 - (-1)^j V_s , \quad (\text{A2})$$

$$v_n = v_i - nV_s/2 - (1 + (-1)^j) V_s/2 . \quad (\text{A3})$$

The profiles φ^{+1} and φ^{-1} are obtained by adding contributions from all j until $1 - T(v_j)$ becomes negligible (note that j starts at zero). The transmissivities are approximated as $T(v_n) = [1 + 0.75\tau(v_n)]^{-1}$. Assuming a Holtsmark function (Lang 1974), $\tau(v_n)$ is the line opacity away from line center (by the amount $\lambda_0 v_n/c$) due to the opacity of either the precursor (n even) or of the shell (n odd). The line center opacities τ_0^p are derived from N_{21}^{prec} (if $p = +1$) and N_{21}^{mir} (if $p = -1$). The attenuation of the transmissivity due to dust absorption has been taken into account by determining the column density of dust crossed by the resonant photon at each passage across the discontinuity (assuming that reflection takes place at a geometrical depth such that $\tau(v_n) \approx 1$). As in NM88, we neglect the diffusion in frequency that results from scattering within the static material on either side of the shock front.

B. Comparison with NM88

The position of the peak intensity within the Fermi accelerated profile, V_7^{peak} , shifts towards the blue as N_{21}^{mir} and/or V_7^s are progressively increased. Our numerical calculations lead to the following relation valid only when $N_{21}^{\text{mir}} \gg 0.002(V_7^s)^2$:

$$V_7^{\text{peak}} \simeq 5.82 (1 + \delta) \left(V_7^s N_{21}^{\text{mir}} \right)^{\frac{1}{3}} , \quad (\text{B1})$$

with δ defined as:

$$\delta = 0.16 (N_{21}^{\text{mir}})^{-\frac{1}{3}} \sqrt{V_7^s} , \quad (\text{B2})$$

where $100 V_7^{\text{peak}} \text{ km s}^{-1}$ is the peak intensity velocity. This expression assumes that $N_{21}^{\text{prec}} = N_{21}^{\text{mir}}$. When $N_{21}^{\text{mir}} \gtrsim 10^4$ (that is, for a negligible δ), the above expression for V_7^{peak} becomes identical to that of NM88. A more general expression is to appear in Joguet & Binette (1998).

REFERENCES

Joguet, B., & Binette, L. 1998, A&A, in preparation

Binette, L., Wang, J. C. L., Zuo, L., & Magris, G. 1993, AJ, 105, 797

Bonilha, J. R. M., Ferch, R., Salpeter, E. E., Slater, G., & Noerdlinger, P. D. 1979, ApJ, 233, 649

Ferruit P., Binette, L., Sutherland, R. S., & Pécontal, E. 1997, A&A, 322, 73

Lang, K. R. 1974, in Astrophysical formulae, Springer Verlag, Berlin

Neufeld, D. A., & McKee, C. F. 1988, ApJ, 331, L87 (NM88)

Rees, M. J. 1989, MNRAS, 239, 1P

Tenorio-Tagle, G. 1979, A&A, 71, 59

van Ojik R. 1995, PhD thesis, Leiden University (The Netherlands)

van Ojik, R., Röttgering, H. J. A., Carilli, C. L., Miley, G. K., Bremer, M. N., Macchetto, F. 1996, A&A, 313, 25 (vO96)

van Ojik R., Röttgering, H. J. A., Miley, G. K., & Hunstead, R. W. 1997, A&A, 317, 358

TABLE 1
PARAMETERS CHARACTERIZING PROFILES φ^{+1} , φ^{-1} OF FIG. 1.

Model	V_7^s	N_{21}^{sou}	N_{21}^{mira}	T_2^{sou}	T_2^{mir}	μ_D ^b
a	3.0	0.01	0.1	1.0	1.0	0
b	3.0	0.2	0.2	1.0	1.0	0
c	3.0	0.1	1.0	1.0	1.0	0
d	3.0	1.0	1.0	1.0	1.0	0
e	3.0	5.0	1.0	1.0	1.0	0
f	3.0	1.0	0.1	1.0	1.0	0
g	3.0	0.1	0.01	1.0	1.0	0
h	3.0	0.1	0.001	1.0	1.0	0
i	3.0	3.0	1.0	1.0	1.0	0
j	3.0	3.0	1.0	1.0	1.0	0.2 ^c
k	3.0	0.0002	1.0	100	1.0	0
l	3.0	0.28	0.53	1.0	1.0	0

^aWe have set $N_{21}^{prec} = N_{21}^{mir}$ in all the above calculations.

^bThe dust-to-gas ratio within the two mirrors relative to the local interstellar value ($\mu_D=1$).

^cThe fraction of Ly α absorbed by dust within the two mirrors is 63%.

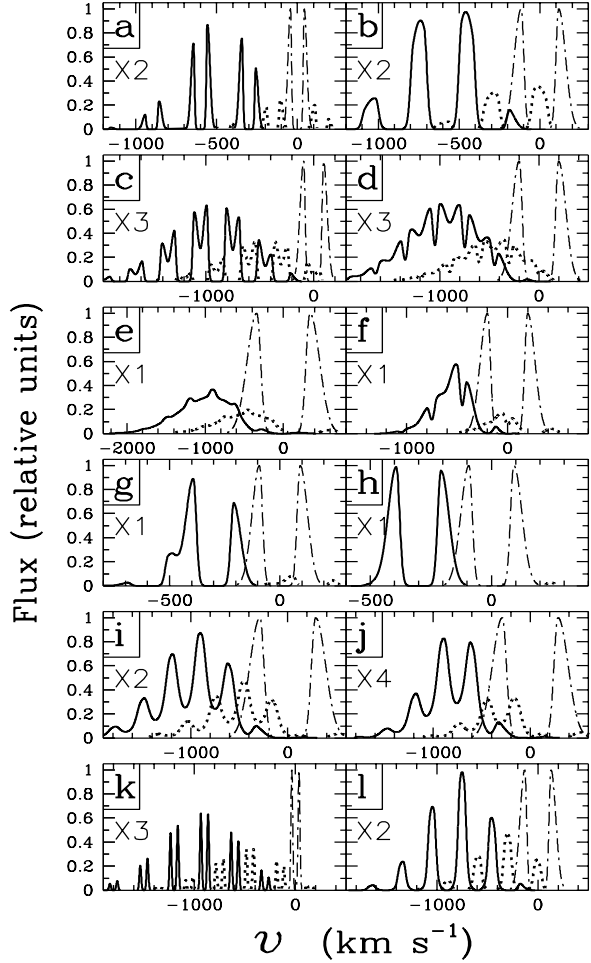


Fig. 1.— The dash-dotted line represents different double-horned source profiles (cf. § 2.1) as a function of velocity from line center ($v = c(\lambda - \lambda_0)/\lambda_0$). The profiles resulting from Fermi acceleration were calculated using the parameters given in Table 1. After multiplication by an appropriate constant (e.g. X4, to provide better comparison with the source profile), they are plotted according to the observer’s perspective: front (φ^{+1}): solid line or back (φ^{-1}): dotted line.

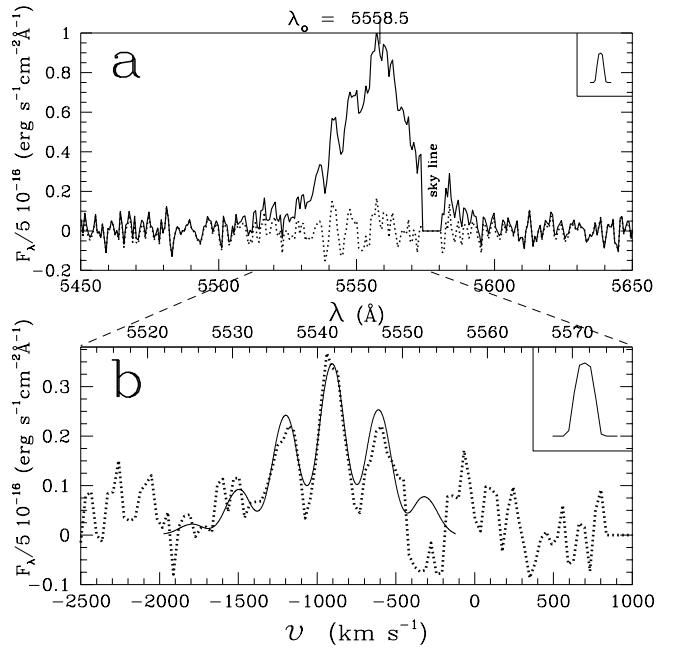


Fig. 2.— *Top:* The observed Ly α profile of 1243+036 (solid line). The dotted line represents the high frequency structures extracted by smoothing and subtraction. *Bottom:* The difference between the left half and the smoothed and folded right half of the Ly α profile is shown as dotted line. The lower ordinate is the velocity shift if we adopt as line center $\lambda_0 = 5558.5\text{\AA}$. The solid line represents the Fermi acceleration of the Ly α profile of an H II region in its champagne phase. This profile has been convolved by the instrumental profile shown in the inset boxes.